Morphological Study of Two-Phase Polymer Blends During Compounding in a Novel Compounder on the Basis of Elongational Flows

Michel Bouquey,[1] Cyril Loux,[1] René Muller,[1] Gilles Bouchet[2]

[1]*Laboratoire d'Ingénierie des Polymères pour les Hautes Technologies, Equipe d'Accueil Conventionnée 4379, Ecole Européenne de Chimie, Polymères et Matériaux, Université de Strasbourg, 25 Rue Becquerel, F67000 Strasbourg, France*
[2]*Institut de Mécanique des Fluides et des Solides, Université de Strasbourg/Centre National de la Recherche Scientifique, 2 Rue Boussingault, F67000 Strasbourg, France*

Received 27 January 2010; accepted 15 April 2010
DOI 10.1002/app.32645
Published online 27 July 2010 in Wiley Online Library (wileyonlinelibrary.com).

ABSTRACT: A new laboratory-scale mixing device based on an original concept was built and tested. This device has important technical features such as tightness to liquids and gases, the possibility of direct specimen molding after mixing, and easy handling of reactive systems. In comparison with existing laboratory mixers, the flow in this mixer is characterized by a high contribution from elongational flow. Morphological data on model polystyrene/poly(methyl methacrylate) blend systems have proved the high distributive and dispersive mixing efficiency in comparison with a classical rotational batch mixer. The influence of different experimental parameters such as the flow rate, mixing time, mixing element geometry, and viscosity ratio of blends is characterized and discussed. Much finer dispersions have been obtained with this new device versus those obtained with a conventional mixer with equivalent specific energy input. © 2010 Wiley Periodicals, Inc. J Appl Polym Sci 119: 482–490, 2011

Key words: computer modeling; mixing; particle size distribution; polymer blends; processing

INTRODUCTION

Most properties of multiphase polymer systems, including immiscible (i.e., two-phase) polymer blends, are intimately related to their morphology.[1–3] More specifically, the importance of rheology–morphology relationships in two-phase polymer blends has been emphasized since the 1970s in a series of articles by Han and coworkers,[4–9] van Oene,[10] and Vinogradov et al.[11] At the same time, since the pioneering work of Taylor,[12] the elongation and breakup mechanisms of dispersed droplets in flow have been extensively studied.[13,14] In particular, the influence of the flow geometry on the critical capillary number, which controls the drop deformation process, has been described.[15,16] One of the main conclusions of these studies is the higher efficiency of elongational flow with respect to shear flow, at given values of the capillary number and the viscosity ratio (p; i.e., the viscosity of the dispersed phase over the matrix viscosity), for elongating and breaking dispersed droplets. However, most data on elongational flow have been obtained with extensional rheometers[17–19] or four-roll mill geometry;[20] these are difficult to use in an industrial mixing process for molten polymer blends. Therefore, in most studies, the investigated binary blends have been prepared either in a twin-screw extruder[21] or in an internal batch mixer,[22–24] in which shear flows are predominant.

The idea of promoting elongational flow during mixing with the objective of enhancing the dispersive mixing efficiency came up recently, and several devices are described in the literature.[25–27] In particular, Meller and coworkers[28–30] studied the deformation and breakup of dispersed droplets in molten polymer blends of different viscosities. They used a capillary rheometer equipped with dies with different entry profiles and showed that the mixing efficiency in the converging flow zone was dependent both on the shape of the convergence and on the volume flow rate (Q).

The use of convergent (and divergent) elongational flow to enhance the efficiency of mixing in an industrial process has been limited up to now, mainly because of the high pressure drops that arise if several convergent/divergent flow units are associated in series (e.g., at the exit of a continuously operated extruder).[28,31] On the other hand, the flow between two opposite chambers through a small-

Correspondence to: M. Bouquey (bouqueym@ecpm.u-strasbg.fr).

diameter die was first described by Hausman[32,33] and was later used by Westofer[34] to measure the pressure dependence of the viscosity of a polymer melt. Mackley et al.[35] adapted this geometry to design their so-called multipass rheometer, in which the influence of the number of passes through the central die on the rheological properties can be studied. Recently, Son[36] showed that the concept of the multipass rheometer can be adapted to design a batch mixer in which an unlimited number of convergent/divergent flows can be applied to the material to be mixed.

In this article, we describe a new mixing device[37] based on the geometry of Mackley's multipass rheometer, the design of which was significantly modified with respect to Son's microcompounder to allow original operation modes. The efficiency of our device as a mixer was tested on model immiscible polystyrene (PS)/poly(methyl methacrylate) (PMMA) blends, for which easy and accurate morphology characterization by transmission electron microscopy (TEM) is possible. A volume finite numerical simulation of the flow within the mixer was carried out with the objective of explaining the high distributive and dispersive mixing capability of the device.

DESCRIPTION OF THE COMPOUNDER

The recently built device, which we call RMX (for elongational flow reactor and mixer), is schematically represented in Figure 1. The material to be mixed is alternately pushed from one cylindrical chamber to the other through a central static mixing element by two reciprocally moving pistons. For all results presented in this article, the mixing element was composed of a small-diameter cylindrical die. The convergent and divergent elongational flows at the entrance and exit of the die are expected to contribute significantly to dispersive mixing. The following original features characterize the RMX device.

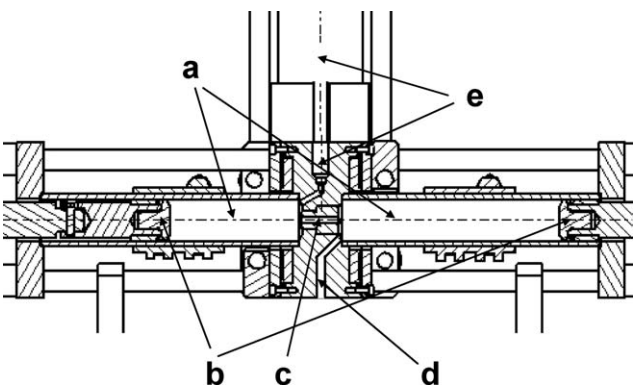

Figure 1 Schematic drawing of the mixing device: (a) mixing chambers, (b) pistons, (c) mixing element, (d) feeding unit and feeding channel, and (e) outlet channel (sampling or molding).

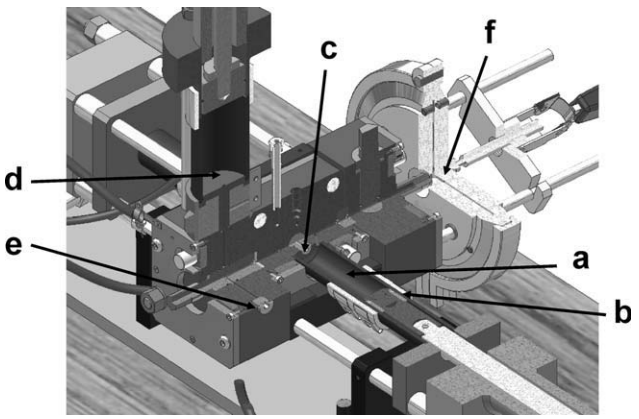

Figure 2 Three-dimensional view of the mixer: (a) chamber, (b) piston with seal, (c) mixing element, (d) feeding unit for melts, (e) feeding channel for liquids, and (f) mold.

Feeding of the components

In addition to the central channel connecting the chambers (the mixing channel), the mixing element is fitted with three additional channels: one for the feeding of the components to be mixed, another for the outlet of the mixed material, and a third one (not represented in Fig. 1) that connects one of the chambers to a pressure transducer. The feeding channel can be connected to a feeding unit, which allows the melting of pellets and the feeding of the obtained melt into the mixer. It can also be connected to a three-way sieve and a pump, which allows the direct feeding of low-viscosity liquids

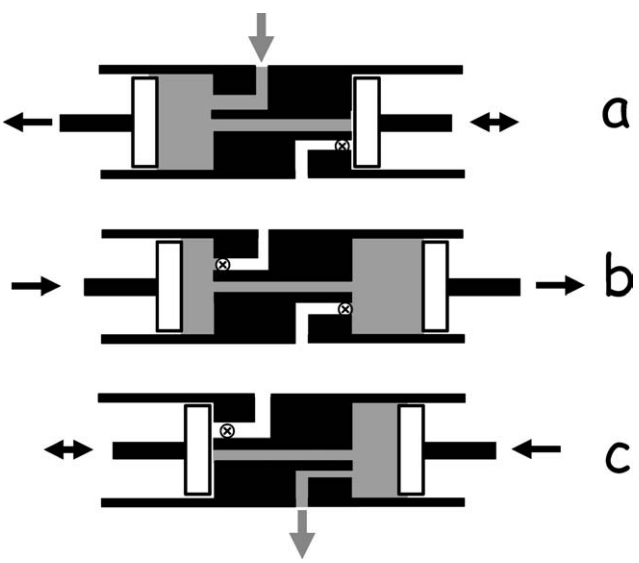

Figure 3 Schematic operation of the mixer.

(see Fig. 2). The feeding of a component into the mixer is schematically represented in Figure 3(a): the material flows through the feeding channel into the chamber on the left side, and a small counter pressure is applied to the corresponding piston, which moves back until the total volume of the material is reached. At the same time, the piston in the opposite chamber is in a fixed position and thus prevents the material from flowing to the right through the mixing channel. Most simply, if all components to be mixed are in the form of pellets, a mixture of the pellets can be introduced into the feeding unit, and after melting, the material is introduced into the mixer according to sequence 3a. However, it is also possible to sequentially feed several components. For instance, two mutually reactive components (A and B) can be independently fed into the mixer in the following way. Component A is introduced first according to step 3a. It is then transferred into the right chamber through the mixing channel by the displacement of the left piston. Component B is introduced according to step 3a; the left piston, moving back again, and the right piston, remaining in a fixed position, thus prevent component B from flowing into the left chamber and minimize the area of the A/B interface before the mixing step begins.

Mixing

Figure 3(b) schematically represents the reciprocal displacement of the pistons during the mixing step. At this time, both the feeding and outlet channels are closed. The volume of material inside the mixer is adjusted by the initial positions of the pistons and can be varied in the range of 10–100 cm^3. The pistons are hydraulically driven by a servovalve at a controlled speed in the range of 0.18–180 mm/s, which for 3-cm-diameter pistons corresponds to Q values in the range of 0.125–125 cm^3/s. The maximum pressure in the upstream chamber is limited by the power of the hydraulic station and is therefore a function of Q. Typically, at the highest Q value, the upstream pressure can reach around 150 bars. A mixing sequence is defined by the piston velocity (v; or Q) and the number of cycles (N), and an experiment can be composed of several consecutive sequences at different Q values. The pressure in one of the chambers is continuously measured during the mixing sequence by a pressure transducer (Dynisco pressure range of 0–700 bars) connected to this chamber through the mixing element. Because the flow is reversed during each cycle, only one pressure transducer is required to measure the pressure drop between the two chambers; as a matter of fact, the transducer measures alternately the upstream and downstream pressures at each flow reversal, so the pressure drop between the chambers is merely the difference of both pressure measurements.

Outlet of the mixed material

At the end of the mixing step, all material is first pushed into the right chamber connected to the outlet channel. As shown in Figure 3(c), the outlet channel can be used to take samples at the end of an experiment (or even during an experiment between two mixing sequences) or can be connected to a mold (see also Fig. 2). During molding, the left piston is in a fixed position, and the right piston pushes the material into the mold. During this step, the device works like an injection machine. Unlike other types of microcompounders (the twin-screw type or Brabender type), no additional step (e.g., recovering the melt, placing it into a mold, reheating it, and molding it) is therefore required to mold specimens of specified shapes after mixing. Figure 4 shows a typical mold geometry for both tensile and melt rheology test specimens.

Moreover, the central part of the mixing element is removable, so the shape and diameter of the central mixing channel can be easily varied. In this study, we tested two different mixing channel geometries corresponding to two dies with different length-to-diameter (L/D) ratios: a long-die mixing element (LDME) with $L = 15$ mm and $D = 3$ mm ($L/D = 5$) and a short-die mixing element (SDME) with $L = 3$ mm and $D = 2$ mm ($L/D = 1.5$). The dimensions have been chosen so that the ratio D^4/L is almost the same in both elements; as a result, the pressure drop through the die is the same at a constant Q value for a Newtonian material. Finally, the mixer can be made pressure-tight by appropriate seals between the pistons and the chambers, so it can in principle be operated as a stirred pressurized reactor. This operation mode is discussed later.

EXPERIMENTAL

Materials

Commercial grades of PS (Polystyrol 143E, BASF, Ludwigshafen; Germany) and PMMA (ACRIGEL, Resarbras da Bahia S.A., Sao Bernardo do Campo, Brazil) were used to prepare the binary blends. These polymers were completely immiscible under the conditions considered here. Their interfacial tension at 210°C, the temperature at which the blending tests were carried out, was determined with the fiber retraction method[38] to be equal to 1 ± 0.1 mN/m. Similar values were obtained via the fitting of the Palierne model of viscoelastic emulsions[39] to linear viscoelastic data for blends of known particle size distributions.[40,41] The values of the shear viscosity at 210°C as a function of the shear rates of both PS and PMMA were determined with a cone and plate (ARES 2000, TA Instruments) and capillary rheometry and are shown in Figure 5. The ratio of the

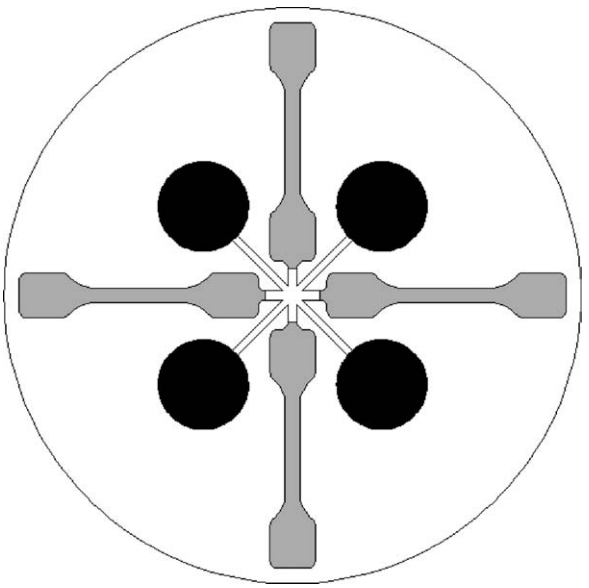

Figure 4 Example of the mold used in the RMX (25-mm diameter disks and dog-bone-shaped specimens, ISO 527-2-5A).

viscosity of PMMA to that of PS was nearly constant and was equal to approximately 4.5 in the whole range of shear rates.

Preparation of the blends

Two blend compositions were investigated in this study: 10/90 (w/w) PS/PMMA, for which p was equal to 0.22 (low-viscosity droplets dispersed in a higher viscosity matrix), and 90/10 (w/w) PS/PMMA, for which p was equal to 4.5 (high-viscosity droplets dispersed in a lower viscosity matrix). The components were filled into the mixers in the form of a dry blend of pellets.

The morphologies of the blends obtained with the RMX device with two different mixing elements (long-die and short-die geometries) were compared to those obtained with an internal batch mixer (a Haake Rheomix 600 (Thermo-Fischer, Karlsruhe, Germany) equipped with counter-rotating, roller-type blades). The initial temperature at the beginning of the mixing step was set to 210°C for all tests. Depending on the mixing conditions, a temperature rise due to viscous heating was observed, and the temperature could reach approximately 20°C.

Depending on the mixing device, the influence of the following processing parameters was investigated.

RMX

For each blend composition and each mixing element, blends were realized at Q values of 3.5, 7, and 14 cm^3/s, which corresponded to v values of 5, 10, and 20 mm/s, and with different N values ranging from 10 to 200, which corresponded to different mixing times (t). For a typical material volume of approximately 35 cm^3, the duration of a complete cycle was 5–20 s. The design of the mixer made it possible to take samples through the outlet channel with increasing values of N with the same initial amount of material. The sampling procedure was therefore particularly easy and fast. For the sake of comparing morphologies obtained with different devices and different mixing elements, it is useful to estimate the specific mechanical energy input during the mixing process. For the RMX device, this quantity (W_{sp}^{RMX}) can be simply expressed as follows:

$$W_{sp}^{RMX} = \frac{\Delta P \times Q \times t}{m} \quad (1)$$

where ΔP is the pressure drop between the upstream and downstream chambers and m is the total mass of material in the mixer. Because the pressure is continuously measured during the test in one of the chambers, the pressure drop can be easily determined by the difference in pressure during one reciprocation. On the other hand, the specific energy input can also be expressed as a function of N and v: for the lowest value of Q, the wall shear rate in the die ($\dot{\gamma}_w$) is of the order of

$$\dot{\gamma}_w = \frac{4Q}{\pi R^3}\frac{3n+1}{4n} \quad (2)$$

where R is the die radius and n is the flow rate index, which, according to Figure 5, is close to 0.25 for both polymers at shear rates higher than approximately 100 s^{-1}. The lowest value of the wall shear rate, as determined with Eq. (2), is of the order of 2000 s^{-1}, and this confirms that a power-law equation can be used for the relation between Q and the pressure drop for all experiments in this study. The total mixing time (t) can be expressed as a function of N:

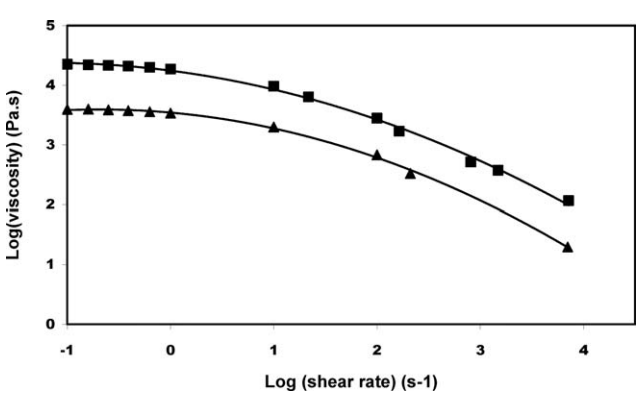

Figure 5 Viscosities at 210°C for (■) PMMA and (▲) PS.

$$t = \frac{Nm}{\rho Q} \tag{3}$$

where ρ is the mass density. For a power-law fluid, the pressure scales as Q^n. Therefore, the specific energy scales as follows:

$$W_{sp}^{RMX} = \frac{\Delta P \times N}{\rho} \propto v^n N \tag{4}$$

Rheomix 600 batch mixer

For each blend composition, blends were realized at three different rotation speeds (50, 100, and 150 rpm) and three different t values [5, 10, and 15 min (measured after the end of the filling step)]. The specific mechanical energy input during the mixing process ($W_{sp}^{Rheomix}$) is easily expressed as follows:

$$W_{sp}^{Rheomix} = \frac{\Omega T t}{m} \tag{5}$$

where Ω is the rotation speed (rad/s) and T is the torque (N m).

Because the flow geometry and, in particular, the relative importance of elongational flow were completely different in the two mixers and in the two mixing elements of the RMX, the obtained morphologies were compared with a constant specific energy input.

Morphological characterization

At the end of the mixing step, the material was cooled to room temperature. TEM (Hitachi Science Systems, Ltd, Ibaraki, Japan) at 60 kV was used to characterize the particle size distribution within the blends; 50- and 80-nm cuts were prepared with a Leica EM Ultracut 6 microtome equipped with diamond knives. For the PS/PMMA system, the phases were clearly identified by TEM, with the PS phase appearing dark and the PMMA phase appearing white. For each sample, at least three cuts taken at several positions were analyzed, and the particle size distribution was determined with image analysis software (Aphelion) from micrographs corresponding to 40 × 40 μm^2 domains. The number-average particle diameter (D_n) and volume-average particle diameter (D_v) values were discussed only on a comparative basis as a function of mixing conditions and were therefore directly determined from these micrographs without any correction like the Schwartz–Saltikov correction, which is often used for polymer blends.[42]

NUMERICAL SIMULATION

A numerical simulation of the flow within the RMX mixer was carried out with the objective of characterizing the relative importance of elongational and shear flows. The flow was assumed to be axisymmetric, and the volume within both chambers and in the mixing element was discretized with a structured

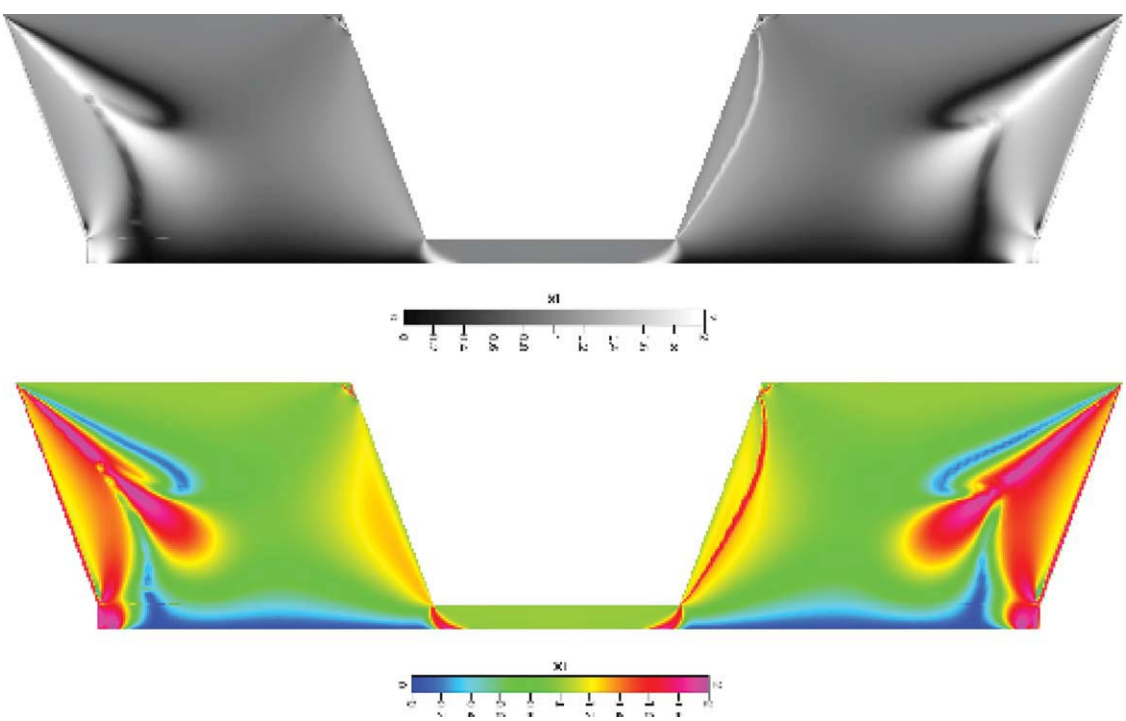

Figure 6 Mapping of the flow by Astarita's parameter. [Color figure can be viewed in the online issue, which is available at wileyonlinelibrary.com.]

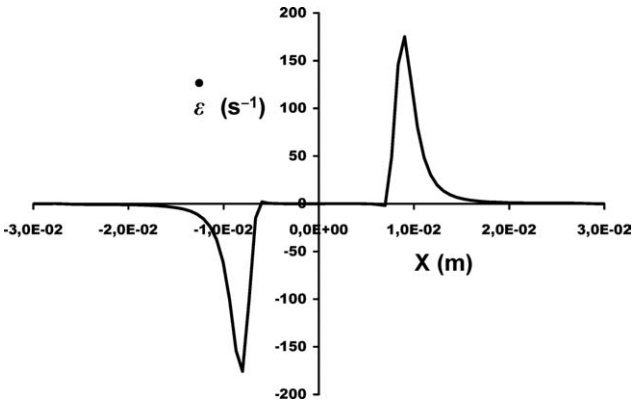

Figure 7 Elongation rate dv/dy (s^{-1}) on the axis versus the position (m).

mesh. A nonslip boundary condition was imposed on the walls and surface of the pistons, and the pistons moved with a constant velocity parallel to the axis. The total volume was conserved during the simulation. To solve this problem, we used a finite volume code (CFD-ACE) that allowed us to solve the continuity and Navier–Stokes equations for an incompressible fluid.[43] From the viscosity/shear rate curves in Figure 5, the parameters of a Carreau-type equation were identified for each polymer and taken into account in the simulation under the assumption that the material followed a generalized Newtonian equation of state.[44] Because the geometry was in motion, remeshing of the volume was required at each time step. The solver compressed the cells on one side and expanded them on the other side. The mesh displacement was taken into account in the calculations with the ALE method (simple interpolation).

The flow geometry was characterized by a scalar parameter (χ) defined by Astarita:

$$\chi = 2\frac{\Omega_{rel}}{\Omega_{rel} + D} \tag{6}$$

where D is the magnitude of the strain rate tensor and Ω_{rel} is the magnitude of the relative rate of the rotation tensor ($\Omega - \mathbf{W}$, where Ω is the vorticity tensor and $\mathbf{W}$ is the tensor giving the rate of rotation of the eigenvectors of D). With this definition, χ is an objective quantity whose values are in the range of 0–2. $\chi = 0$ corresponds to pure elongational flow, $\chi = 1$ corresponds to simple shear flow, and $\chi = 2$ corresponds to rigid body motion.

Figure 6 shows a mapping of Astarita's parameter (χ) in the volume of the mixer with the LDME. As expected, the flow was nearly elongational in the contraction and expansion zones close to the mixing element and was purely simple shear in the die of the mixing element.

Once the velocity field was determined, we could also estimate the mapping of the elongational strain rate in the convergent and divergent zones. The values along the axis of symmetry are shown in Figure 7 for $v = 1$ cm/s ($Q = 7$ cm^3/s). Very high values of the elongational strain rate were found close to the mixing element, but the corresponding residence times were very short because of increasing fluid velocity. Because of the strong gradients of the strain rate, it would be difficult to compare the particle sizes obtained with our mixer to data obtained either experimentally[14] or theoretically[12] in steady flow.

A further objective of the numerical simulation was to explain the high distributive mixing efficiency of the RMX device during the first cycles of the mixing step; this was also observed by Son.[36] This issue will be the topic of a forthcoming article and will not be further discussed here.

RESULTS AND DISCUSSION

Influence of N (RMX)

Whatever the blend composition (10/90 or 90/10), the geometry of the mixing element, or the value of v was, approximately 20 cycles at least were necessary to obtain a dispersion-type morphology. As shown in Figure 8(a), for a 10/90 PS/PMMA blend obtained with the LDME and a v value of 10 mm/s, after 10 cycles, a complex morphology with large PS domains containing PS inclusions was observed. After 40 cycles [Fig. 8(b)], a dispersion-type morphology was obtained, for which the average particle diameters could be determined. A general observation for all mixing conditions was a rapid initial decrease in the particle size with N or the energy input. Most often, the average particle values reached a plateau, which indicated a steady-state blend morphology. On the other hand, small particles were present from the early steps of the mixing process, and increasing N led to the progressive breakup of the largest particles and to a reduction of the particle size polydispersity.

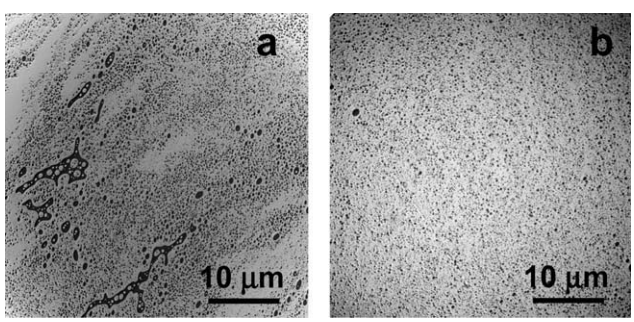

Figure 8 TEM micrographs for two different N values for the 10/90 PS/PMMA LDME ($v = 10$ mm/s): (a) 10 and (b) 20.

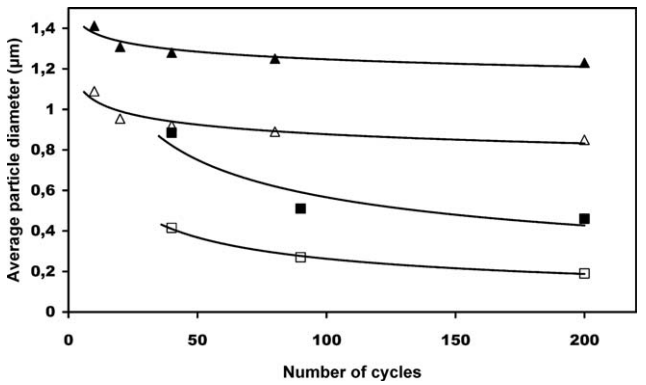

Figure 9 D_n and D_v (μm) versus N for 90/10 PS/PMMA (v = 10 mm/s, temperature = 210°C): (□) LDME D_n, (■) LDME D_v, (△) SDME D_n, and (▲) SDME D_v.

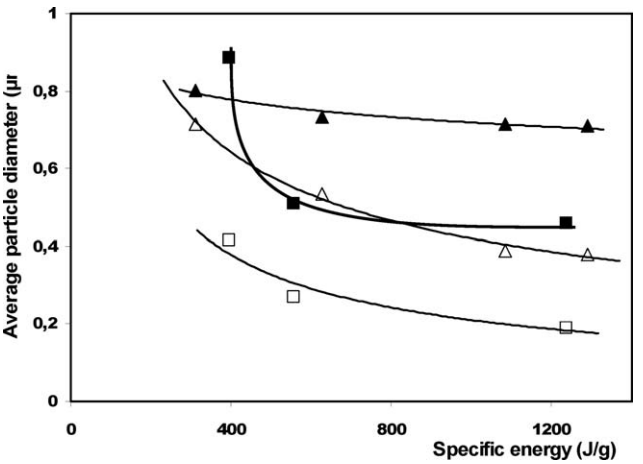

Figure 10 D_n and D_v (μm) versus the specific energy input (J/g; 90/10 PS/PMMA, v = 10 mm/s, temperature = 210°C): (□) LDME D_n, (■) LDME D_v, (△) Haake Rheomix D_n, and (▲) Haake Rheomix D_v.

Influence of the geometry of the mixing element (RMX)

Figure 9 shows the variation of D_n and D_v with N for 90/10 PS/PMMA blends obtained at v = 10 mm/s in the two mixing elements (SDME and LDME). The LDME led to a much finer dispersion, which indicated that the shear flow within the die played an important role in the breakup process. This result can be understood by the assumption that the droplets, elongated in the upstream contraction flow, required a certain time to break up (e.g., by filament instability). For a short die, the residence time was very small, and we could assume that the elongated droplets reached the divergent flow zone in the downstream chamber before breakup and therefore eventually recovered their initial size. On the other hand, a longer residence time in a long die could allow the breakup process to take place within the die and, consequently, smaller average particle sizes.

The values of the pressure drop at the same value of Q were not too different in the two mixing elements because of their diameters and lengths. Therefore, when the data in Figure 9 were plotted as a function of the specific energy input instead of N, the respective positions of the curves for the LDME and SDME were unchanged, and the aforementioned conclusions still held true.

Comparison of the morphologies of the blends obtained with the RMX with the LDME and with the Haake Rheomix internal batch mixer

Figure 10 shows the values of D_n and D_v as a function of the specific energy input for 90/10 PS/PMMA blends obtained in the RMX with the LDME at v = 10 mm/s and in the Haake Rheomix internal batch mixer at 100 rpm. With equivalent energy input, a finer dispersion was obtained with the RMX, and this could be attributed to the higher elongational flow component. It should be recalled that for the blend considered here, p is equal to 4.5, and for this value, the critical capillary number in simple shear becomes infinite;[14] this confirms the

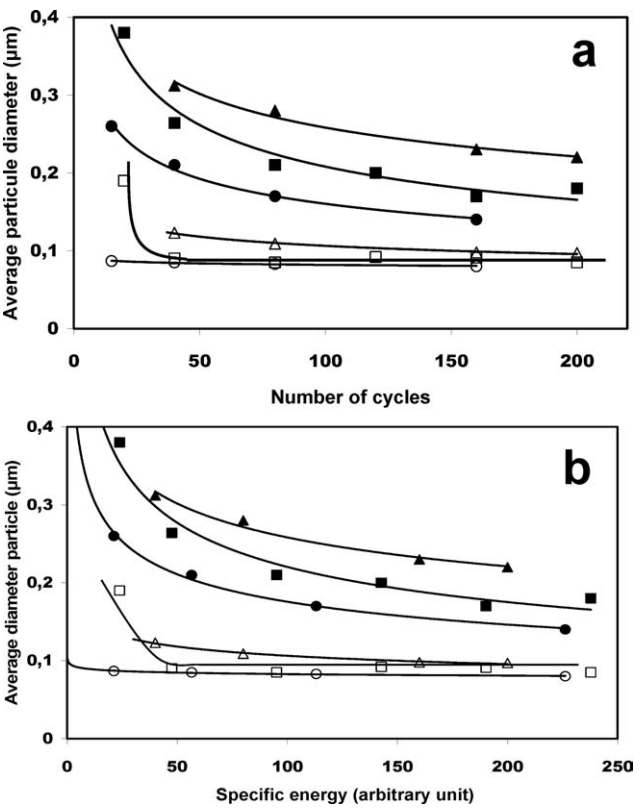

Figure 11 D_n and D_v (μm) versus (a) N and (b) the specific energy input (J/g; 10/90 PS/PMMA, RMX LDME at different v/Q values, temperature = 210°C): (△) D_n at 5 mm/s, (▲) D_v at 5 mm/s, (□) D_n at 10 mm/s, (■) D_v at 10 mm/s, (○) D_n at 20 mm/s, and (●) D_v at 20 mm/s.

importance of the elongational flow component in the breakup process.

Influence of Q and p

In Figure 11(a), the morphological data are plotted at different Q values and at different v values (5, 10, and 20 mm/s) as a function of N for 10/90 PS/PMMA blends obtained in the RMX LDME. The first remark concerns p, which for this blend is equal to 0.22. The experimental results confirm that for equivalent experimental conditions, a better dispersion is obtained than that for the 90/10 PS/PMMA system, for which p is 4.5: $D_v \cong 0.2$ μm and $D_n \cong 0.1$ μm for $p = 0.22$ and $D_v \cong 0.45$ μm and $D_v \cong 0.2$ μm for $p = 4.5$ at $v = 10$ mm/s. This result was expected from the literature.[14,45]

The second result, which comes from the data in Figure 11(a), concerns the influence of Q and N on D_n and D_v, respectively: as soon as N exceeded approximately 50, D_n was almost independent of Q and t and had a very small value of approximately 0.1 μm. On the other hand, D_v decreased both with N up to at least 200 cycles and with Q. This result is again in agreement with a breakup mechanism based on droplet elongation and further breakup by interfacial instability. This mechanism produced a significant number of very small droplets even in the early stages of blending that were responsible for the small initial values of D_n. The later decrease in D_v was attributed to remaining larger drops that broke up progressively as t increased.

Finally, the data in Figure 11(a) were plotted in Figure 11(b) via the rescaling of the x axis as $N \times (v/10 \text{ mm/s})^n$ according to Eq. (4); this amounts to the plotting of the data as a function of the specific energy input. No significant changes appeared in the respective positions of the curves, and the previous discussion remained valid when the morphological data were reconsidered as a function of the energy input.

CONCLUSIONS

A new laboratory-scale mixing device (RMX) has been built and tested. It has original technical features such as tightness to liquids and gases, the ability to easily feed melts and low-viscosity liquids into the mixing chamber, and the possibility of sampling and directly molding specimens after mixing (this allows easy handling of reactive systems). In comparison with existing laboratory mixers, the flow in the RMX device is characterized by a high contribution from elongational flow.

The results of this article demonstrate the efficiency of RMX versus a commercial laboratory-scale mixer. Its efficiency for dispersive mixing is attributed to the combination of elongational flow in the convergent zone and shear flow in the die of the mixing element. For a die with $L/D = 5$, the size distribution of dispersed domains in model PS/PMMA blends obtained in the RMX is typically reduced by a factor of 2 with respect to blends obtained with the same specific energy input with a Haake Rheomix 600 mixer. The influence of the following parameters on the size distribution of dispersed particles has been characterized and discussed: N, Q through the mixing element, the L/D ratio of the mixing channel, and the dispersed phase over matrix p. The following conclusions can be drawn. The morphology reaches a steady state with increasing energy input or t after typically 50 to 100 cycles. v or Q through the mixing element has a significant effect on the morphology: with a constant energy input, the average particle size continuously decreases with increasing Q. The L/D ratio of the mixing channel has a major effect on the final morphology; much finer morphologies are obtained for $L/D = 5$ than for $L/D = 1.5$, and this indicates that the combination of extensional flow in the chambers and shear flow in the channel plays an important role in the dispersion process. Finally, the results confirm that high-viscosity droplets ($p > 1$) are more difficult to disperse that low-viscosity droplets ($p < 1$), but in all case, the elongational flow mixer leads to better results for the size distribution than a rotary mixer with an equivalent specific energy input.

A still open issue that is currently being investigated by numerical simulation is the efficiency of the RMX for distributive mixing. Several sources of flow irreversibility during the cyclic mixing process have been identified even at very low Reynolds numbers, and these results will be published in a separate article.

Finally, because of the possibility of working under a controlled atmosphere and high pressures, the RMX has a broad field of potential applications. It can, in particular, be operated as a chemical batch reactor for polymer modification with volatile reactants or even for polymerization. Moreover, the design of the mixing element allows continuous feeding and an outlet, and this makes possible its use as a stirred continuous reactor.

The authors thank Ines Souilem, Julien Bonnet, and Jerome Rondin for the preparation of the blends mixed in the RMX device and in the Haake Rheomix internal batch mixer. They also thank Badi Triki for performing some of the analyses by TEM.

References

1. Yu, W.; Bousmina, M.; Zhou, C. X.; Tucker, C. L. J Rheol 2004, 48, 417.

2. Han, C. D. Rheology in Polymer Processing; Academic: New York, 1976.
3. Han, C. D. In Multiphase Flow in Polymer Processing; Press, A., Ed.; Kluwer Academic Publishers, New York, 1981; Chapter 4.
4. Han, C. D.; Yu, T. C. J Appl Polym Sci 1971, 15, 1163.
5. Han, C. D.; Yu, T. C. Polym Eng Sci 1972, 12, 81.
6. Han, C. D.; Kim, Y. W. Trans Soc Rheol 1975, 19, 245.
7. Han, C. D.; Kim, Y. W. J Appl Polym Sci 1975, 19, 2831.
8. Han, C. D.; Kim, Y. W. J Appl Polym Sci 1976, 20, 2905.
9. Han, C. D. J Appl Polym Sci 1975, 19, 2403.
10. van Oene, H. J Colloid Interface Sci 1972, 40, 448.
11. Ablazova, T. I.; Tsenbrenko, M. B.; Yudin, A. B.; Vinogradov, B. V. J Appl Polym Sci 1975, 19, 1799.
12. Taylor, G. I. Proc R Soc Lond 1932, 138, 834.
13. Min, K.; White, J. L.; Fellers, J. F. J Appl Polym Sci 1984, 29, 2117.
14. Grace, H. P. Chem Eng Commun 1982, 14, 225.
15. Elmendorp, J. J.; Vandervegt, A. K. Polym Eng Sci 1986, 26, 1332.
16. Palierne, J. F. Rheol Acta 1990, 29, 204.
17. Delaby, I.; Ernst, B.; Muller, R. J Macromol Sci Phys B 1996, 35, 547.
18. Delaby, I.; Ernst, B.; Muller, R. Rheol Acta 1995, 34, 525.
19. Delaby, I.; Ernst, B.; Germain, Y.; Muller, R. J Rheol 1994, 38, 1705.
20. Milliken, W. J.; Leal, L. G. J Non-Newtonian Fluid Mech 1991, 40, 355.
21. Utracki, L. A.; Shi, Z. H. Polym Eng Sci 1992, 32, 1824.
22. Ait-Kadi, A.; Marchal, P.; Choplin, L.; Chrissemant, A. S.; Bousmina, M. Can J Chem Eng 2002, 80, 1166.
23. Bousmina, M.; Ait-Kadi, A.; Faisant, J. B. J Rheol 1999, 43, 415.
24. Lee, J. K.; Han, C. D. Polymer 1999, 40, 6277.
25. Maric, M.; Macosko, C. W. Polym Eng Sci 2001, 41, 118.
26. Harvey, A. P.; Mackley, M. R.; Stonestreet, P. Ind Eng Chem Res 2001, 40, 5371.
27. Luciani, A.; Utracki, L. A. Int Polym Process 1996, 11, 299.
28. Meller, M.; Luciani, A.; Manson, J. A. E. Int Polym Process 1999, 14, 221.
29. Meller, M.; Luciani, A.; Sarioglu, A.; Manson, J. A. E. Polym Eng Sci 2002, 42, 611.
30. Meller, M.; Luciani, A.; Manson, J. A. E. Polym Eng Sci 2002, 42, 634.
31. Tokihisa, M.; Yakemoto, K.; Sakai, T.; Utracki, L. A.; Sepehr, M.; Li, J.; Simard, Y. Polym Eng Sci 2006, 46, 1040.
32. Hausman, J. M. U.S. Pat. 2,813,300 (1957).
33. Hausman, J. M. U.S. Pat. 2,948,920 (1960).
34. Westofer, R. E. Soc Plast Eng Trans 1961, 1, 153.
35. Mackley, M. R.; Marshall, R. T. J.; Smeulders, J. J Rheol 1995, 39, 1293.
36. Son, Y. J Appl Polym Sci 2009, 112, 609.
37. Terrisse, J.; Bouquey, M.; Muller, R. Fr. Pat. WO02008142234 (2007).
38. Carriere, C. J.; Birsaw, G.; Sammler, R. L. Rheol Acta 2000, 39, 476.
39. Palierne, J. F. Rheol Acta 1991, 30, 497.
40. Graebling, D.; Muller, R.; Palierne, J. F. Macromolecules 1993, 26, 320.
41. Graebling, D.; Muller, R.; Palierne, J. F. J Phys Iv 1993, 3, 1525.
42. Corte, L.; Leibler, L. Polymer 2005, 46, 6360.
43. Ryssel, E.; Brunn, P. O. J Non-Newtonian Fluid Mech 1999, 86, 309.
44. Bird, R. B.; Wiest, J. M. Annu Rev Fluid Mech 1995, 27, 169.
45. Manas-Zloczower, I. In Mixing and Compounding of Polymers: Theory and Practice; Hanser, Munich, 2009; Chapter 3.